Data-driven spatio-temporal dynamic brain connectivity analysis using fALFF: Application to sensorimotor task data

Khondoker Murad Hossain*‡, Suchita Bhinge*, Qunfang Long*, Vince D. Calhoun† and Tülay Adali*§
*Dept. of CSEE, University of Maryland Baltimore County, Baltimore, MD 21250
†Tri-institutional Center for Translational Research in Neuroimaging and Data Science (TReNDS), Georgia State University, 55 Park Pl NE, Atlanta, GA 30303
Email: hossain10@umbc.edu‡, adali@umbc.edu§

***Abstract*—Dynamic functional connectivity (dFC) analysis enables us to capture the time-varying interactions between brain regions and can lead to powerful biomarkers. Most dFC studies are focused on the study of temporal dynamics and require significant postprocessing to summarize the results of the dynamics analysis. In this paper, we introduce an effective framework that makes use of independent vector analysis (IVA) with fractional amplitude of low frequency fluctuation (fALFF) features extracted from task functional magnetic resonance imaging (fMRI) data. Our approach, which is based on IVA with fALLF features as input, (IVA-fALLF) produces an effective summary of the dynamics also greatly facilitating the study of both spatial and temporal dynamics in a more concise manner. IVA-fALLF captures the spatial and temporal dynamics of sensorimotor task data and identifies a component with significant difference in dynamic behavior between healthy controls (HC) and patients with schizophrenia (SZ). We also demonstrate aberrant behavior in the brain networks of patients with SZ as they show more variability and less consistency than HC. Finally, our post analysis using behavioral scores finds significant correlation between brain imaging data and the associated behavioral scores, increasing confidence on our results. Our results are consistent with the previous data-driven dFC analysis as we find similar brain networks showing abnormal behavior in patients with SZ. Moreover, our analysis identifies component behavior in task and rest windows separately and provides additional confirmation of results through correlation with behavioral scores.**

***Index Terms*—Independent vector analysis (IVA), fractional amplitude of low frequency fluctuation (fALFF), sensorimotor (SM) task data, dynamic functional connectivity, behavioral scores**

I. Introduction

The human brain consists of functionally connected regions that interact continuously with each other. Static connectivity analysis cannot capture time-varying interactions across brain networks while dynamic connectivity analysis has been successfully used to capture dynamic patterns from healthy controls and patients with a variety of disorders [1]–[6]. Unusual functional connectivity has helped us to identify various disorders such as schizophrenia [7]-[10], bipolar disorder [11], generalized anxiety disorder [12], attention deficit hyperactivity disorder [13] and mild cognitive impairment [14].

Most dynamic functional connectivity (dFC) investigation procedures only consider the temporal dependence of the brain regions while overlooking the connectivity of the spatial regions. Few of the studies that analyze changes in spatial networks can be broadly categorized as model or data driven. Model-driven methods make stronger assumptions about the nature of the data, such as in-region of interest (ROI) based methods make use of pre-defined brain networks [15]-[17]. Data-driven methods such as independent component analysis (ICA) can extract brain networks with minimal prior assumptions and have been used to study dynamics [18]-[19]. Independent vector analysis
(IVA) extends ICA to multiple datasets [20]-[21] and can effectively capture the variability in both the spatial and temporal directions. Ma et al., [1] and Bhinge et al., [22]-[23] used resting state fMRI data with IVA to study dynamics using a windowed approach. One issue with the application of IVA for dynamics studies is the fact that as the number of datasets increases, precision of IVA can be compromised [23]-[24]. In addition, study of dynamics primarily consider use of resting state data [1], [22]-[23] while cognitive tasks require responses from participants and a dynamic analysis can show how brain networks evolve with the task [19] and provides synchrony among subjects. The amplitude of low frequency fluctuation (ALFF) approach has been used as an effective summary in a number of studies such as [25]-[26]. In this paper, we introduce the use of fractional ALFF (fALFF) features using task fMRI data for studying spatial and temporal dynamics using IVA. This effectively alleviates the dimensionality issue in IVA and provides another important advantage in summarizing the dynamics. In general, in dynamics studies, following the extraction of spatial and/or temporal maps, summary of dynamics is obtained using a number of post-processing steps [1], [22]-[23], [27]. Our approach based on IVA with fALLF features as input also produces an effective summary of the dynamics also greatly facilitating the study of spatial and temporal dynamics in a more concise manner.

We use a sensorimotor (SM) data collected from 147 healthy

This work was supported in part by the National Institute of Biomedical Imaging and Bioengineering under Grant R01EB020407, National Science Foundation under Grant 1631838, and National Science Foundation- Computing and Communication Foundations under Grant 1618551.

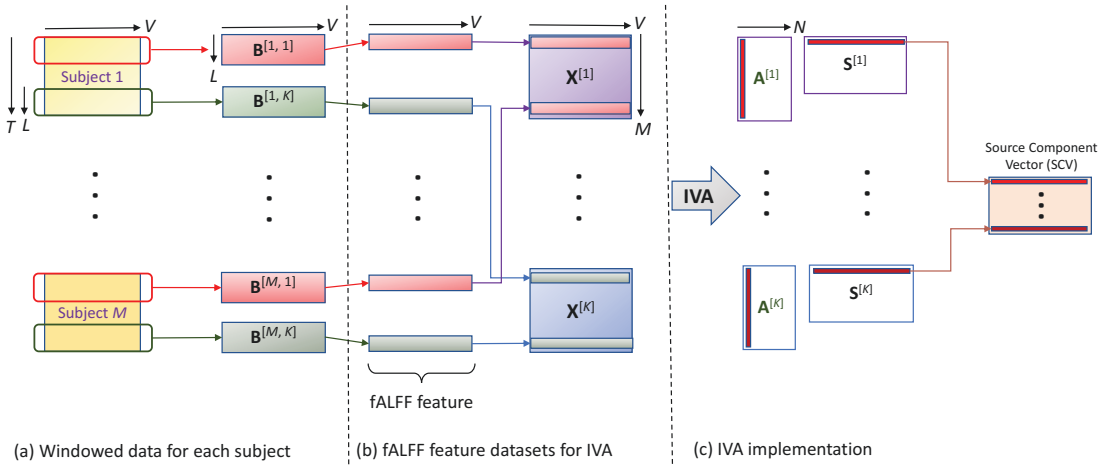

Fig. 1. IVA framework for capturing dynamic brain activity using fALFF features. (a) Windowing fMRI data with no overlap for task-rest blocks. (b) Extracting fALFF features for the windowed data. Each windowed fALFF for all the subjects are concatenated together form one dataset. (c) IVA is used to capture the dynamics.

controls (HC) and 106 patients with schizophrenia (SZ). We show that the proposed IVA framework with fALLF captures both the spatial and temporal changes successfully. We identify a motor component with significant difference between HC and SZ across the windows. Component variability and consistency are also reported to illustrate the differences for the two components. These results clarify that brain networks of patients with SZ show more fluctuation and less consistency than those of healthy controls during the task. We also perform a post analysis using behavioral scores and identify a number of behavioral variables that significantly correlate with the subject variations extracted using IVA, further increasing our confidence on the final results.

The remainder of the paper is organized as follows. Section II presents the fALFF feature extraction and background of IVA. It also shows the proposed IVA framework that we use to capture the dynamics. Section III shows the implementation details and results on the feature data. Section IV provides a discussion of the results and points out future directions.

II. Materials and Methods

A. Dataset

We use the MIND Clinical Imaging Consortium (MCIC) dataset (publicly available at http://coins.trendscenter.org) comprised of 253 participants: 147 healthy controls (HC) and 106 patients with schizophrenia (SZ) with an age range of 18 to 60 years [28]. The dataset consists of fMRI scans collected from both HC and SZ groups while performing a sensorimotor task from four sites: the University of New Mexico (UNM), the University of Minnesota (UMinn), Massachusetts General Hospital (MGH) and the University of Iowa (UIowa).

The task captures the auditory and somatosensory response with the change of audio tones of different frequencies. Subjects were presented with a sequence of auditory stimuli consisting of 16 different tones each lasting 200 ms and ranging in frequency from 236 Hz to 1,318 Hz with a 500 ms inter-stimulus interval. The first tone presented was set at the lowest pitch and each subsequent tone was higher than the previous one until the highest tone was reached, at which point the order of the tones were reversed. Each tonal change required a button press with the right thumb. A total of 15 increase-and-decrease blocks were alternated with 15 rest (fixation) blocks, with each block lasting 16 seconds in duration.

The fMRI images were collected on a 3-T Siemens Trio scanner in UMinn, UIowa and MGH where UNM used a Siemens 1.5-T Sonata scanner. For all sites prospective acquisition correction (PACE) corrected, whole-brain, single-shot EPI data parallel to the AC-PC line (in-plane resolution 3.4 mm, 27 slices, slice thickness = 4 mm, 1 mm skip, slice order interleaved, TE = 30 ms for 3T, TE = 40 ms for 1.5T, TR = 2 s, FA= 90, FOV = 22 cm, 3DDAs (dummy data acquisition), bandwidth = 3126Hz/pixel) were acquired.

The fMRI data was preprocessed using an automated analysis pipeline [29] carried out in SPM. The pipeline consisted of: 1) aligning all the images with the first image as the reference using INRIalign approach [30] to correct minor motion of the subject; 2) correcting for time differences between the slices using the middle slice as the reference; and 3) spatial normalization to MNI space, including reslicing to $3 \times 3 \times 3mm^3$, resulting in $53 \times 63 \times 46$ voxels. Data were then spatially smoothed with a 10-mm FWHM Gaussian filter. The preprocessed fMRI data is masked to remove the non-brain voxels using the Group ICA of fMRI Toolbox (GIFT) [31]. After masking the dimension of the fMRI data for each subject is $120 \times 67,747$ (number of timepoints(T) $\times$ number of voxels(V)).

B. Data windowing and fALFF feature extraction

We propose a three stage framework to use fALLF features in our dynamic study. The detailed framework is shown in Figure 1.

In the first stage, a sliding-window approach is used to divide the data into task and rest windows. Each window is of length $L = 8$ time points (16 seconds) as both task and rest block consists of 8 time points. We exclude the first 5 time points as the first auditory stimulation (task) window starts from $T = 6$. $\mathbf{B}^{[m,k]} \in \mathbb{R}^{L\times V}$, denotes the kth window of the mth subject, where M $(m = 1, ..., 147$ are HC and $m = 148, ..., 253$ are SZ) is the number of subjects and K is the number of windows. Windowing the data results in $K = 14$ windows (from $T = 6$ to 117) with no overlap and with alternating task-rest blocks. fALFF maps are computed using the REST software (http://resting-fmri.sourceforge.net) on the windowed data. To compute the fALFF features, windowed data is first transformed to the frequency domain and then sum of the frequencies in the low frequency band $(0.01 - 0.15$ Hz) is obtained. For each voxel, the ratio of the averaged square root of the power spectrum within the $0.01 - 0.15$ Hz frequency band to that of the entire detectable frequency range is calculated. In the second stage, the fALFF features computed for all the subjects for one window are concatenated together, yielding $K = 14$ datasets as shown in Figure 1.

We perform dimension reduction by applying PCA on the feature dataset and retaining N principal components. We denote the dimension reduced dataset as $\mathbf{X}^{[k]} \in \mathbb{R}^{N\times V}$ and use 90% as the threshold for the variance preserved which gives us order $N = 40$.

C. IVA and the model for dynamics

ICA is a blind source separation technique which decomposes a given set of observations into a mixing matrix and sources by assuming that observed data is generated from a linear mixture of independent sources [32]. It has proven effective in fMRI data analysis [33]-[34], however it is designed for a single dataset. Independent vector analysis (IVA) is an extension of ICA to multiple datasets which enables the use of statistical dependence of latent (independent) sources across datasets by exploiting both second order and higher order statistics [35].

Given K datasets, each consists of V samples, each dataset is a linear mixture of N independent sources,

$$\mathbf{x}^{[k]}(v) = \mathbf{A}^{[k]}\mathbf{s}^{[k]}(v), 1 \le k \le K, 1 \le v \le V, \qquad (1)$$

where, $\mathbf{A}^{[k]} \in \mathbb{R}^{N\times N}$, $k = 1, ..., K$ denotes the invertible mixing matrix. For a given set of observations, IVA generative model can be written as, $\mathbf{X}^{[k]} = \hat{\mathbf{A}}^{[k]}\mathbf{S}^{[k]}$. $\mathbf{X}^{[k]} \in \mathbb{R}^{N\times V}$ denotes the observations and $\mathbf{S}^{[k]} \in \mathbb{R}^{N\times V}$ are the latent sources. IVA estimates K demixing matrices, $\mathbf{W}^{[k]}, k = 1, ..., K$ so that the dataset specific sources can be estimated as, $\hat{\mathbf{S}}^{[k]} = \mathbf{W}^{[k]}\mathbf{X}^{[k]}$.

The demixing matrices are estimated such that the following IVA cost function is minimized,

$$\mathcal{J}_{\text{IVA}} = \sum_{n=1}^{N}\left[\sum_{k=1}^{K}\mathcal{H}(\hat{s}_n^{[k]}) - \mathcal{I}(\hat{\mathbf{s}}_n)\right] - \sum_{k=1}^{K}\log\left|\det(\mathbf{W}^{[k]})\right| \qquad (2)$$

IVA defines a source component vector (SCV) as, $\hat{\mathbf{s}}_\mathbf{n} = \left[\hat{s}_n^{[1]}, ..., \hat{s}_n^{[K]}\right]^T \in \mathbb{R}^K$, where $\hat{s}_n^{[K]}$ is the nth component of the kth dataset. $\mathcal{I}(\hat{\mathbf{s}}_n)$ denotes the mutual information of the nth SCV. The entropy, $\mathcal{H}(\hat{s}_n^{[k]})$ and mutual information term balance the independence within the dataset and dependence across the datasets by minimizing the IVA cost.

Application of IVA on the fALFF feature dataset, $\mathbf{X}^{[k]}, k = 1, ..., K$, results in maximally independent components (ICs), $\mathbf{S}^{[k]}, k = 1, ..., K$. We obtain the subject-specific spatial maps, using dual regression [31], which are denoted as $\mathbf{s}_n^{[m,k]}$, meaning nth IC of mth subject in kth window. The estimated mixing matrices, $\hat{\mathbf{A}}^{[k]}$, are back reconstructed to obtain dataset-specific mixing matrices, $\mathbf{A}^{[k]}, \in \mathbb{R}^{M\times N}$, using, $\mathbf{A}^{[k]} = (\mathbf{D}^{[k]})^{-T}\ \hat{\mathbf{A}}^{[k]}$, where $\mathbf{D}^{[k]}$ is the data reduction matrix. The reduction matrix, $\mathbf{D}^{[k]}$, comprises of the N eigenvectors, corresponding to the first N largest eigenvalues of the covariance matrix of $\mathbf{X}^{[k]}$. Each column of $\mathbf{A}^{[k]} \in \mathbb{R}^{M\times N}$, indicated as $\mathbf{a}_n^{[k]}, n = 1, ..., N$, represents the weight of the corresponding source $\mathbf{s}_n^{[k]}$ on each subject. It quantifies each subject's contribution to the ICs and hence is referred to as subject covariations of the ICs.

In this study, we use an IVA implementation which combines two IVA algorithms: IVA-G [20] and IVA-L-SOS [23]. IVA-G takes only second order statistics (SOS) into account by assuming the SCVs are multivariate Gaussian while IVA-L-SOS (IVA-L with SOS) utilizes a multivariate Laplace prior for SCV distribution. IVA-L-SOS takes both SOS and higher order statistics (HOS) into account by calculating the covariance matrix of each SCV and it is a good match for fMRI data. We initialize IVA-L-SOS with a solution from IVA-G to take the advantage of both algorithms.

As IVA is an iterative algorithm, the decomposition results vary from different initialization points. Hence, we use a technique based on cross joint inter-symbol interference (cross-jISI), an extension of the technique proposed in [36] to multiple datasets, in order to select the most consistent IVA run from 30 independent runs with random initializations.

III. Results and Post-Analysis

A. Experimental results

1) Estimated ICs: We obtain $N = 40$ ICs for each of the $K = 14$ windows from IVA. First, we take the Z-score of the ICs which measures the distance of raw scores from population mean in standard deviation units. Then we convert the voxels with Z-score greater than threshold $1.5(|Z| \ge 1.5)$ from MNI coordinates to Talairach coordinates to assign anatomical and functional labels for the left and right hemispheres. Of the 40 ICs we select 8 task-related ICs for our dynamic study from visual inspection. These networks are labeled based on the following classes: default mode network (DMN), sensorimotor (SM), auditory (AUD), cerebellum (CB), motor (MC), medial temporal (MT), visual (VIS) and frontal (FRO). In an IVA decomposition the corresponding estimated ICs across the windows are maximally dependent and they form a SCV together. For a better visualization, we take the mean of each

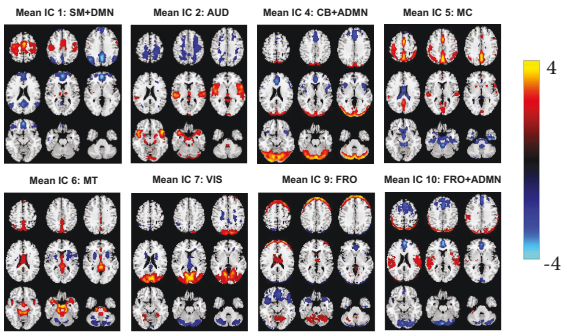

Fig. 2. Spatial maps of the mean ICs are categorized into 8 domains: default mode network (DMN), sensorimotor (SM), auditory (AUD), cerebellum (CB), motor (MC), medial temporal (MT), visual (VIS) and frontal (FRO). Red voxels indicate positive activated and blue voxels indicate negative activated.

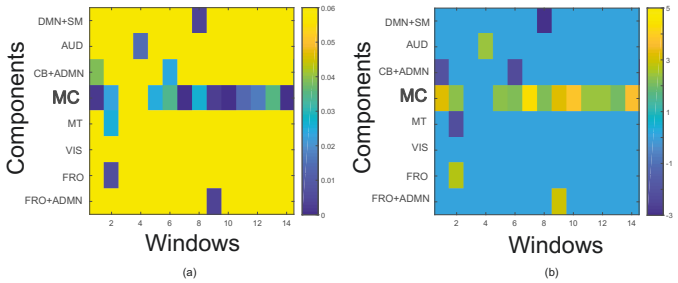

Fig. 3. Dynamic change of group difference for selected ICs. Two sample t-test on the corresponding subject covariations reveals statistically significant difference between the two groups (HC vs. SZ) (a) p-value of components across windows where MC shows group difference in most of the windows. (b) t-value of components across windows where positive t-value means higher activation in HC and negative t-value means higher activation in SZ.

selected IC across the windows and show the spatial maps of the eight mean ICs (mean SCVs) in Figure 2.

2) Dynamics of subject covariation: In order to study the difference in dynamic behavior between healthy controls and patients, we use the subject covariation matrices, $\mathbf{A}^{[k]} \in \mathbb{R}^{M\times N}$, $k = 1, ..., K$ obtained after back reconstructing the mixing matrices from IVA. The values in each column of subject covariation matrices, $a_{mn}^{[k]}$, $n = 1, ..., N, m = 1, ..., M$, quantify the contribution of subjects to each IC.

Dynamics of ICs across windows: We perform a two-sample t-test on subject covariations to identify components that show group difference between the HC and SZ group. We summarize the p-values (a) and t-values (b) of the test results for the 8 ICs across 14 windows in Figure 3. A positive t-value indicates higher activation in HC and a negative t-value means higher activation in SZ. All components except VIS show group difference in at least one window where MC shows group difference in most of the windows hence that advocates our component selection for the dynamic study.

Mean subject covariation across windows for HC and patients: We calculate the mean of subject covariation values for the two groups, HC and SZ, separately to compare their contribution in each IC and show the behavior of subject covariation for the two groups in Figure 4. It depicts a clear on-off pattern in most of the windows as the SM task has a paradigm of task-rest blocks. Two ICs, CB+ADMN and MC, are used for example, as CB+ADMN shows higher intensity for SZ in most of windows and MC shows higher intensity for HC in all the windows. The asterisk indicates that the subject covariation yields significant difference between the two groups in that particular window. These plots provide complementary information of the dynamics of subject covariation.

B. Quantification of dynamics

A quantitative study of the spatio-temporal imaging features can help identify unique biomedical patterns of SZ. Component variability and functional connectivity are features that have been individually investigated in previous studies [1], [23]. In this paper, we use two metrics, component variability and component consistency to study the difference between HC and SZ regarding dynamics.

1) Component similarity: We study how each component fluctuates across the windows by investigating the component similarity. For subject m it is computed as follows,

$$r_m = |\text{corr}(\mathbf{s}_n^{[m,k]}, \mathbf{s}_n^{[m,k+1]})| \tag{3}$$

i.e., r_m is the absolute value of Pearson's correlation coefficient between the nth component at window k, $\mathbf{s}_n^{[m,k]}$ and nth component at window $k+1$, $\mathbf{s}_n^{[m,k+1]}$. A higher value of this metric suggests that the spatial network is less variable. Figure 5(a) shows the results for the components that demonstrate significant differences ($p < 0.05$) between HC and SZ. The DMN+SM, AUD, MC, MT and FRO+ADMN component shows less variability in HC. SM and MC were also identified less variable among HC in previous dynamic study as SZ patients show deficit in perception and motor regions.

2) Component consistency in task and rest blocks: In order to compare the difference of dynamics between HCs and SZs during task and rest separately, we define a metric, component consistency. For the nth component we compute the absolute Pearson's correlation coefficient for all pairwise combinations of task windows and all pairwise combinations of for rest windows separately. We repeat this process for all M subjects which gives us the component consistency in task windows and rest windows. Figure 5(b), 5(c) shows that all the selected components except FRO+ADMN are significantly consistent for HC in task, but in rest only DMN+SM, AUD and MC show significant consistency in HC compare to SZ. The results illustrate that dynamic behavior of the participants change with task and rest where brain networks of HC show a better organized or more regular change between states.

C. t-maps of the ICs

To summarize the change in spatial maps, we perform both one sample and two sample t-test on the spatial maps of each IC for HCs and SZs either with the task and rest windows. As shown in Figure 6(a), 6(b), both CB+ADNN and VIS

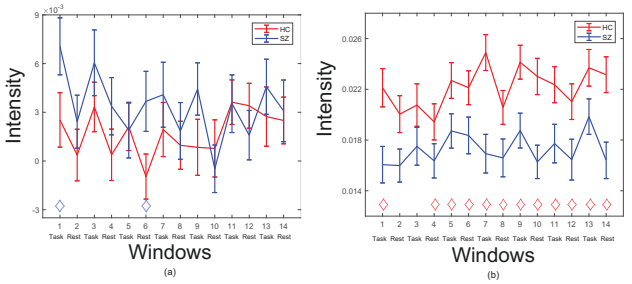

Fig. 4. Mean subject covariation across windows for HC and patients. (a) change of subject covariation in CB+ADMN with time. (b) change of subject covariation in MC with time. Asterisk means group different in a particular window where blue diamond (◇) means significantly higher intensity in SZ and red diamond (◇) means significantly higher intensity in HC.

yield significant difference between HC and SZ in terms of the number and location of activated voxels. Interestingly, CB+ADNN shows more significant difference in task windows and VIS shows more significant difference in rest windows.

D. Behavioral scores

Along with brain imaging data, behavioral scores have been used recently to study the aberrant behavior in SZ [28], [37]-[38]. A total of 51 behavioral variables (BVs) were available for 253 subjects. We show how our previous results help to identify unique biomedical behaviors in SZ.

First, we consider one BV as a distinct feature, each feature is of length m, the number of subjects for a correlation study between spatial maps and the BVs. Hence, we calculate the Pearson's correlation coefficient between each feature and average subject covariation across all windows for each of the selected ICs and select 8 features that show the highest correlation. The eight BVs are: Wechsler Adult Intelligence Scale (WAIS-III) [39], Benton Visual Retention Test (BVRT) [40], Wechsler Memory Scale-III (WMS-III) [39] , Hopkins Verbal Learning Test-Revised (HVLT) [41], Grooved Pegboard Test (GP) [42], California Computerized Assessment Package (CalCap)and F-A-S verbal test. We concatenate the behavioral scores as the 15$^{\text{th}}$ dataset, yielding $E = 15$ datasets, $\mathbf{X}_{\text{behav}}^{[e]} \in \mathbb{R}^{P\times M}, e = 1, ..., E, E = 15, P = 8, M = 247$. We perform a second level IVA-G on the 15 datasets to validate a interpret our results.

After the decomposition, we check the correlation structure of SCVs where 15$^{\text{th}}$ row corresponds to the correlation between features extracted from the behavioral scores and one IC across the windows. We perform a two sample t-test to calculate the group difference between HC and SZ in all the SCVs and only show the results for SCV3 as it yields the highest group difference. From 3$^{\text{rd}}$ column of the mixing matrix for dataset 15, $[\mathbf{A}_{\text{behav}}^{[e]}]^T \in \mathbb{R}^{P\times P}, e = 1, ..., E, E = 15, P = 8$ we calculate the contribution of the behavioral scores to SCV3. WMS-3, WMS-3 delay and GP are the most dominant one as shown in Table I where WMS-3, WMS-3 delay are highly associated with working and visual memory and GP is associated with motor functions. Regarding the components, we measured the mean of the 3$^{\text{rd}}$ column of $\mathbf{A}_{\text{behav}}$, across dataset= 1,...,14 and see MC, CB+ADMN, FRO+ADMN are the ones contributing most in SCV3 than other ICs. MC is related to motor activity and CB+ADMN, FRO+ADMN are related to motor and memory functions. From these results, the BVs and spatial maps are showing clear correlation as their associated functions overlap. Also, all the contributing components in SCV3 are related to motor activity which validate our previous results.

TABLE I
CONTRIBUTION OF BEHAVIORAL SCORES AND ICS IN SCV3

Contribution of BVs		Contribution of ICs	
BVs	Percentage of contribution	ICs	Percentage of contribution
WMS-3	30	MC	52
WMS-3 delay	25	CB+ADMN	12
GP	20	FRO+ADMN	10
Other BVs	25	Other ICs	26

IV. DISCUSSION

Recently, time-varying spatial and temporal brain networks have been of great interest in neuroimaging studies. IVA captures the spatio-temporal variability with minimal assumptions but has been applied to a small number of subjects due to the decreased precision when working with large number of datasets. Our proposed IVA framework mitigates this issue as we work with extracted fALFF features from the fMRI data. We use SM task data to identify differences in brain dynamics for SZ patients compared with healthy controls along the time windows. Our framework successfully captures the group difference between HC and SZ without the need for additional post-processing steps. The analysis identifies the networks, SM, MC showing abnormal behavior in SZ as in the previous studies [43]-[44]. SZ shows higher variability than HC as in [1], [23], but in addition, our analysis shows the component variability and consistency both in task and rest windows. Correlation study between the brain networks and behavioral scores yields meaningful correlations. There are a number of important future directions. For example, we can study different overlap of windows as well as window sizes and can further study patient subgroups using the behavioral scores.

V. ACKNOWLEDGEMENT

The hardware used in the computational studies is part of the UMBC High Performance Computing Facility (HPCF). The facility is supported by the U.S. National Science Foundation through the MRI program (grant nos. CNS-0821258, CNS-1228778, and OAC-1726023) and the SCREMS program (grant no. DMS-0821311), with additional substantial support from the University of Maryland, Baltimore County (UMBC). See http://hpcf.umbc.edu for more information on HPCF and the projects using its resources.

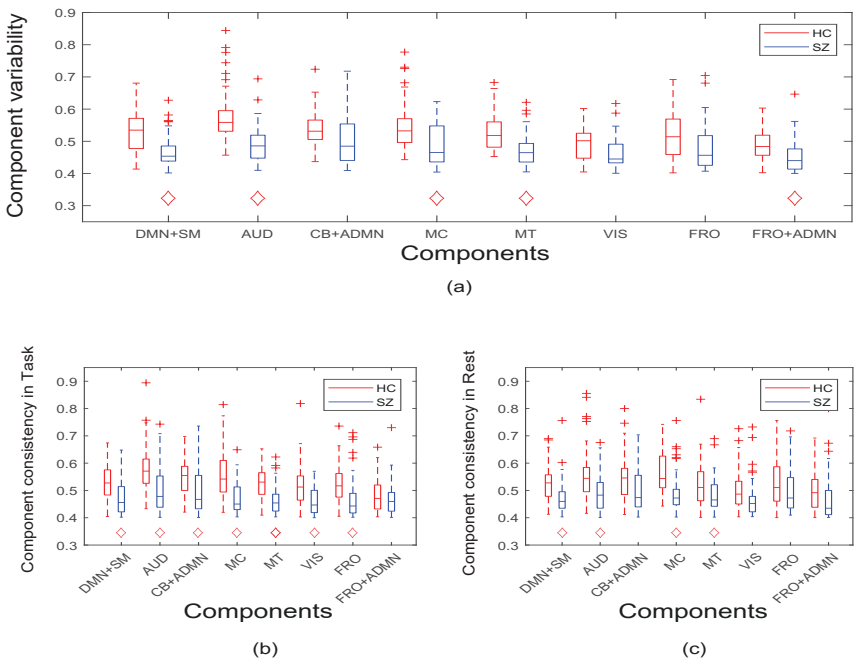

Fig. 5. (a) Component variability of all components. Components that demonstrate significant difference ($p < 0.05$) between HC and SZ group are indicated by a diamond. A red diamond (♢) denotes the corresponding component is significantly less variable in the HC group. The results indicate that DMN+SM, AUD, MC, MT and FRO+ADMN shows significantly less variability in HC. (b-c) Component consistency in task and rest windows. All the selected components except FRO+ADMN are significantly consistent among HC in task but in rest only DMN+SM, AUD and MC shows significant consistency in HC compare to SZ. A red diamond (♢) means components in HC are significantly more consistent.

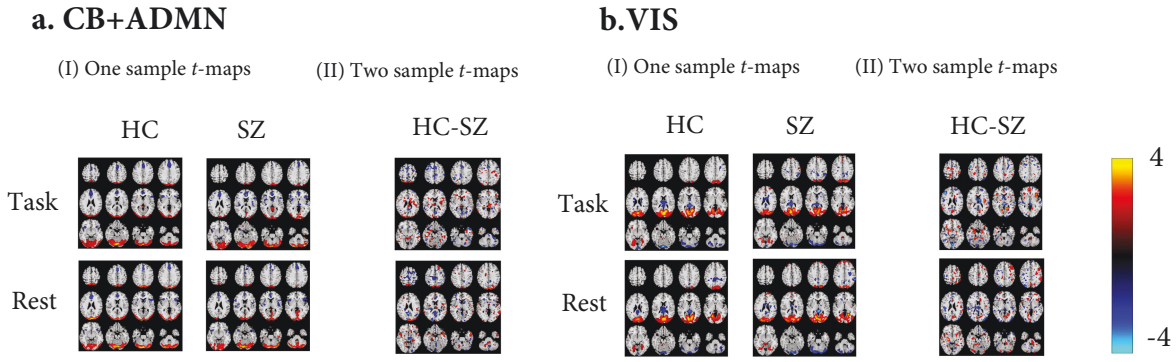

Fig. 6. (a) One sample t-maps and two sample t-maps for CB+ADMN ($p < 0.05$). (I) shows one sample t-maps for HC and SZ both in task and rest. (II) shows two sample t-maps between HC and SZ in task and rest. (b) One sample t-maps and two sample t-maps for VIS ($p < 0.05$). (I) shows one sample t-maps for HC and SZ both in task and rest. (II) shows two sample t-maps between HC and SZ in task and rest.

Omitted Authors Contribution Section as not used in IEEE template.

Shaped Fig 6 from Column to Row to save space.

REFERENCES

[1] S. Ma, V. D. Calhoun, R. Phlypo, and T. Adalı, "Dynamic changes of spatial functional network connectivity in healthy individuals and schizophrenia patients using independent vector analysis," *NeuroImage*, vol. 90, pp. 196–206, 2014.

[2] C. Chang and G. H. Glover, "Time-frequency dynamics of resting-state brain connectivity measured with fMRI," *NeuroImage*, vol. 50, no. 1, pp. 81-98, 2010.

[3] R. M. Hutchison, T. Womelsdorf, E. A. Allen, P. A. Bandettini, V. D. Calhoun, M. Cor-betta, S. Della Penna, J. H. Duyn, G. H. Glover, J. Gonzalez-Castillo et al., "Dynamic functional connectivity: promise, issues, and interpretations," *NeuroImage*, vol. 80, pp. 360–378, 2013.

[4] V. D. Calhoun, R. Miller, G. Pearlson, and T. Adalı,"The chronnectome: time-varying connectivity networks as the next frontier in fMRI data discovery," *Neuron*, vol. 84, no. 2, pp. 262-274, 2014.

[5] V. D. Calhoun and T. Adalı, "Time-varying brain connectivity in fMRI data: whole-brain data-driven approaches for capturing and characterizing dynamic states," *IEEE Signal Processing Magazine*, vol. 33, no. 3, pp. 52-66, 2016.

[6] A. H. C. Fong, K. Yoo, M. D. Rosenberg, S. Zhang, C.-S. R. Li, D. Scheinost, R. T. Constable, and M. M. Chun, "Dynamic functional connectivity during task performance and rest predicts individual differences in attention across studies," *NeuroImage*, vol. 188, pp. 14–25, 2019.

[7] E. Bullmore, S. Frangou, and R. Murray, "The dysplastic net hypothesis: an inte-gration of developmental and dysconnectivity theories of schizophrenia," *Schizophrenia Research*, vol. 28, no. 2-3, pp. 143–156, 1997.

[8] S. M. Lawrie, C. Buechel, H. C. Whalley, C. D. Frith, K. J. Friston, and E. C. John-stone, "Reduced frontotemporal functional connectivity in schizophrenia associated with auditory hallucinations," *Biological Psychiatry*, vol. 51, no. 12, pp. 1008–1011, 2002.

[9] S. Lefebvre, M. Demeulemeester, A. Leroy, C. Delmaire, R. Lopes, D. Pins, P. Thomas, and R. Jardri, "Network dynamics during the different stages of hallucinations in schizophrenia," *Human Brain Mapping*, vol. 37, no. 7, pp. 2571–2586, 2016.

[10] E. Damaraju, E. A. Allen, A. Belger, J. M. Ford, S. McEwen, D. Mathalon, B. Mueller, G. Pearlson, S. Potkin, A. Preda et al., "Dynamic functional connectivity analysis re-veals transient states of dysconnectivity in schizophrenia," *NeuroImage: Clinical*, vol. 5, pp. 298–308, 2014.

[11] B. Rashid, E. Damaraju, G. D. Pearlson, and V. D. Calhoun, "Dynamic connectivity states estimated from resting fMRI identify differences among schizophrenia, bipolar disorder, and healthy control subjects," *Frontiers in Human Neuroscience*, vol. 8, p. 897, 2014.

[12] A. Etkin, K. E. Prater, A. F. Schatzberg, V. Menon, and M. D. Greicius, "Disrupted amygdalar subregion functional connectivity and evidence of a compensatory network in generalized anxiety disorder," *Archives of General Psychiatry*, vol. 66, no. 12, pp. 1361–1372, 2009.

[13] N. de Lacy and V. D. Calhoun, "Dynamic connectivity and the effects of maturation in youth with attention deficit hyperactivity disorder," *Network Neuroscience*, vol. 3, no. 1, pp. 195–216, 2018.

[14] X. Chen, H. Zhang, Y. Gao, C.-Y. Wee, G. Li, D. Shen, and A. D. N. Initiative, "High-order resting-state functional connectivity network for MCI classification,"*Human Brain Mapping*, vol. 37, no. 9, pp. 3282-3296, 2016.

[15] B. Jie, M. Liu, and D. Shen, "Integration of temporal and spatial properties of dynamic connectivity networks for automatic diagnosis of brain disease," *Medical Image Analysis*, vol. 47, pp. 81-94, 2018.

[16] A. Kottaram, L. Johnston, E. Ganella, C. Pantelis, R. Kotagiri, and A. Zalesky, "Spatio-temporal dynamics of resting-state brain networks improve single-subject prediction of schizophrenia diagnosis," *Human Brain Mapping*, vol. 39, no. 9, pp. 3663-3681, 2018.

[17] J. M. Kunert-Graf, K. Eschenburg, D. Galas, J. N. Kutz, S. Rane, and B. W. Brun-ton, "Extracting reproducible time-resolved resting state networks using dynamic mode decomposition," *Frontiers in Computational Neuroscience*, vol. 13, p. 75, 2019.

[18] V. Kiviniemi, T. Vire, J. Remes, A. A. Elseoud, T. Starck, O. Tervonen, and J. Nikkinen, "A sliding time-window ICA reveals spatial variability of the default mode network in time," *Brain Connectivity*, vol. 1, no. 4, pp. 339–347, 2011.

[19] Üsakoglu, G. D. Pearlson, K. A. Kiehl, Y. M. Wang, A. M. Michael, and V. D. Calhoun, "A method for evaluating dynamic functional network connectivity and task-modulation: application to schizophrenia," *Magnetic Resonance Materials in Physics, Biology and Medicine*, vol. 23, no. 5-6, pp. 351–366, 2010.

[20] M. Anderson, T. Adalı, and X.-L. Li, "Joint blind source separation with multivariate gaussian model: Algorithms and performance analysis," *IEEE Transactions on Signal Processing*, vol. 60, no. 4, pp. 1672–1683, 2011.

[21] T. Kim, T. Eltoft, and T.-W. Lee, "Independent vector analysis: An extension of ICA to multivariate components," in *International conference on independent component analysis and signal separation*. Springer, 2006, pp. 165–172.

[22] S. Bhinge, V. D. Calhoun, and T. Adalı, "IVA-based spatio-temporal dynamic connec-tivity analysis in large-scale fMRI data," in *2018 IEEE International Conference on Acoustics, Speech and Signal Processing (ICASSP)*. IEEE, 2018, pp. 965–969.

[23] S. Bhinge, R. Mowakeaa, V. D. Calhoun, and T. Adalı, "Extraction of time-varying spatiotemporal networks using parameter-tuned constrained IVA," *IEEE Transactions on Medical Imaging*, vol. 38, no. 7, pp. 1715–1725, 2019.

[24] Q. Long, S. Bhinge, V. D. Calhoun, and T. Adalı, "Independent vector analysis for common subspace analysis: Application to multi-subject fMRI data yields meaningful subgroups of schizophrenia," *NeuroImage*, p. 116872, 2020.

[25] M. J. Hoptman, X.-N. Zuo, P. D. Butler, D. C. Javitt, D. D'Angelo, C. J. Mauro, and M. P. Milham, "Amplitude of low-frequency oscillations in schizophrenia: a resting state fMRI study,"*Schizophrenia Research*, vol. 117, no. 1, pp. 13-20, 2010.

[26] Z. Yu-Feng, H. Yong, Z. Chao-Zhe, C. Qing-Jiu, S. Man-Qiu, L. Meng, T. Li-Xia, J. Tian-Zi, and W. Yu-Feng, "Altered baseline brain activity in children with adhd revealed by resting-state functional MRI," *Brain and Development*, vol. 29, no. 2, pp. 83–91, 2007.

[27] Z. Fu, Y. Tu, X. Di, Y. Du, G. D. Pearlson, J. A. Turner, B. B. Biswal, Z. Zhang, and V. D. Calhoun, "Characterizing dynamic amplitude of low-frequency fluctuation and its relationship with dynamic functional connectivity: an application to schizophrenia," *NeuroImage*, vol. 180, pp. 619–631, 2018.

[28] R. L. Gollub, J. M. Shoemaker, M. D. King, T. White, S. Ehrlich, S. R. Sponheim, V. P. Clark, J. A. Turner, B. A. Mueller, V. Magnotta et al., "The MCIC collection: a shared repository of multi-modal, multi-site brain image data from a clinical investigation of schizophrenia," *Neuroinformatics*, vol. 11, no. 3, pp. 367–388, 2013.

[29] H. J. Bockholt, M. Scully, W. Courtney, S. Rachakonda, A. Scott, A. Caprihan, J. Fries, R. Kalyanam, J. Segall, R. De La Garza et al., "Mining the mind research network: a novel framework for exploring large scale, heterogeneous translational neuroscience research data sources." *Frontiers in neuroinformatics*, vol. 3, p. 36, 2010.

[30] L. Freire, A. Roche, and J.-F. Mangin, "What is the best similarity measure for motion correction in fMRI time series?" *IEEE Transactions on Medical Imaging*, vol. 21, no. 5, pp. 470–484, 2002.

[31] V. Calhoun and T. Adalı, "Group ica of fMRI toolbox (GIFT)," *Online at http://icatb. sourceforge. net*, 2004.

[32] A. Hyvärinen, P. O. Hoyer, and M. Inki, "Topographic independent component analy-sis," *Neural Computation*, vol. 13, no. 7, pp. 1527–1558, 2001.

[33] V. D. Calhoun, T. Adalı, G. D. Pearlson, and J. J. Pekar, "A method for making group inferences from functional MRI data using independent component analysis," *Human Brain Mapping*, vol. 14, no. 3, pp. 140–151, 2001.

[34] K. Li, L. Guo, J. Nie, G. Li, and T. Liu, "Review of methods for functional brain con-nectivity detection using fMRI," *Computerized Medical Imaging and Graphics*, vol. 33, no. 2, pp. 131–139, 2009.

[35] T. Adalı, M. Anderson, and G.-S. Fu, "Diversity in independent component and vector analyses: Identifiability, algorithms, and applications in medical imaging," *IEEE Signal Processing Magazine*, vol. 31, no. 3, pp. 18–33, 2014.

[36] Q. Long, C. Jia, Z. Boukouvalas, B. Gabrielson, D. Emge, and T. Adalı, "Consistent run selection for independent component analysis: Application to fMRI analysis," in *2018 IEEE International Conference on Acoustics, Speech and Signal Processing (ICASSP)*. IEEE, 2018, pp. 2581-2585.

[37] S. Sponheim, R. Jung, L. Seidman, R. Mesholam-Gately, D. Manoach, D. O'Leary, B. Ho, N. Andreasen, J. Lauriello, and S. Schulz, "Cognitive deficits in recent-onset and chronic schizophrenia," *Journal of psychiatric research*, vol. 44, no. 7, pp. 421–428, 2010.

[38] R. Jin, K. Dontaraju, S.-J. Kim, S. Akhonda, and T. Adalı, "Dictionary learning-based fmri data analysis for capturing common and individual neural activation maps," *IEEE Journal of Selected Topics in Signal Processing*, 2020.

[39] D. Wechsler, *WAIS-3., WMS-3: Wechsler adult intelligence scale, Wechsler memory scale: Technical manual*. Psychological Corporation, 1997.

[40] A. B. Sivan, *Benton visual retention test*. Psychological Corporation San Antonio, TX, 1992.

[41] J. Brandt, "The hopkins verbal learning test: Development of a new memory test with six equivalent forms," *The Clinical Neuropsychologist*, vol. 5, no. 2, pp. 125–142, 1991.

[42] R. M. Ruff and S. B. Parker, "Gender-and age-specific changes in motor speed and eye-hand coordination in adults: normative values for the finger tapping and grooved pegboard tests," *Perceptual and motor skills*, vol. 76, no. 3 suppl, pp. 1219–1230, 1993.

[43] C. Arango, B. Kirkpatrick, and R. W. Buchanan, "Neurological signs and the hetero-geneity of schizophrenia," *American Journal of Psychiatry*, vol. 157, no. 4, pp. 560–565, 2000.

[44] S. M. Silverstein, S. Berten, B. Essex, I. Kovacs, T. Susmaras, and D. M. Little, "An fMRI examination of visual integration in schizophrenia," *Journal of Integrative Neu-roscience*, vol. 8, no. 02, pp. 175–202, 2009.